Sensors & Actuators: A. Physical 378 (2024) 115830

Contents lists available at ScienceDirect

Sensors and Actuators: A. Physical

journal homepage: www.journals.elsevier.com/sensors-and-actuators-a-physical

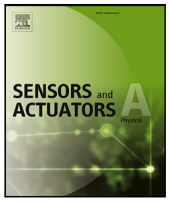

Modular reconfigurable rotary style soft pneumatic actuators

Nicholas Pagliocca, Aatish Gupta, Joshua Knospler, Nand K. Singh, Mitja Trkov *

Department of Mechanical Engineering, Rowan University, 201 Mullica Hill Rd., Glassboro, 08028, NJ, USA

ARTICLE INFO

Keywords:
Soft actuators
Modular robots
Pneumatic actuators
Rotary actuators
Reconfiguration

ABSTRACT

Modular soft robots have the advantage in their ability to be reconfigured and change their morphology on-demand according to a specified task. The actuator design and particularly the inter-unit connectivity strength commonly govern the usability and functionality of these modular robots and their applications. In this paper, we present development of reconfigurable modular rotary soft actuators that allow the construction of highly versatile soft robotic actuators and systems. These pneumatically driven modular actuators are composed of an inner balloon and a flexible arched reinforcement structure to produce a rotary motion. They serve as building blocks which may be combined in various configurations to construct linear assemblies capable of extensile or bending motions. The connection scheme allows for the larger actuators to grow or shrink with the addition or removal of modules. Using finite element simulations and physical characterizations, we systematically explore the mechanical response of individual modular actuators and the role of various connection schemes on their motions upon pressurization. A key conceptual contribution of this work lies in the idea that for a modular soft robotic system, offsetting and tuning actuator alignment relative to an axis of symmetry can lead to substantial changes in mechanical performance. Utilizing these modules we demonstrate the reconfigurability of this modular system by both reconfiguring a large actuator into a pair of smaller actuators that can grasp delicate objects, and reconfiguring actuators to develop a linear crawling robot.

1. Introduction

The abundance and utility of soft robotic actuators has blossomed in recent years. In large part, this is owed to their compliance, low cost, and simple construction. Their compliance fills a void associated with contact safety in less compliant systems making them amenable to many applications in dynamic environments such as materials handling via grippers [1], underwater exploration [2], medical surgeries [3,4], and human-machine interactions [5–7]. Most of the existing soft robots are non-reconfigurable, despite the fact that modular reconfigurable robots are often more versatile and can outperform traditional systems with a fixed morphology [8]. One of the main challenges of modular soft robots is the inter-unit connectivity that should allow easy attachment/detachment of units [9]. As a consequence of these limitations, future advancements of modular soft robots are highly dependent on improving their modularity and reconfigurability through improved actuators and their connection schemes.

Herein, we restrict our discussion and investigation to modular pneumatic soft robotic actuators. The advantage of modular soft robots lies in the capability of tailoring their functionality for on-demand tasks via reassembly or through multiple actuators being chained together [9,10]. Modularity in pneumatic soft actuators has enabled the construction of larger soft robotic systems that can achieve tasks such as locomotion [11,12], human assistance [13], complex motions, such as bending, shrinking, and shearing [14], or even driving a tiny wheeled robot [15].

The actuator design and inter-unit connectivity principles in the existing soft modular robots commonly govern the usability and functionality of these robots and their applications. Some of the existing passive inter-unit connections include permanent- or electro-magnets [12,16], flexible suckers [17], simple plastic connectors [14], and chemical bonding of multi-material interfaces [18]. Each connection scheme offers unique advantages and disadvantages. To elaborate, the limitations of chemical bonding often include long set times to form bonds (sometimes on the order of hours/days), magnet-based connectors have limited strength, suckers are known to be hard to disconnect, and plastic connectors may leak at the soft-rigid material interface. Most often, the connectors are either mechanical or magnetic, where the mechanical connection schemes are noted for high precision and reliability. The downside of mechanical connectors is that their rigid enclosure reduces system compliance and adds mechanical complexity. Several promising mechanical connection schemes exist that scale well to more complicated soft robotic systems. For example, modularized

* Corresponding author.
E-mail address: trkov@rowan.edu (M. Trkov).
URL: https://go.rowan.edu/mtrkov (M. Trkov).

https://doi.org/10.1016/j.sna.2024.115830
Received 31 May 2024; Received in revised form 17 August 2024; Accepted 20 August 2024
Available online 22 August 2024

design blocks for easy assembly using threaded or press fit connectors were developed in [19] and shown to be effective. Enabling quick and easy reconfiguration is a key need for on-demand task execution and successful adoption of modular robots. Connection schemes similar to the recloseable fasteners developed in [20] might offer a potential solution that enables quick reconfiguration and preserves compliance at interfaces, but suffers from connection accuracy.

Modular soft robots are commonly constructed from dedicated, non-universal modules governing their motion (i.e., bending, twisting, extension) and universal connectors for connecting modules and accessories [20,21]. The development of universal soft actuator modules, whose local response is near uniform to one another, with an appropriate inter-module connection schemes, would enable simplified soft robot assembly and scalable representation of complex global deformations. For instance, actuators composed of origami shells and perforated sheets that exhibit highly tailored capabilities and complex motions [22,23] offer a semi universal solution as their inflatable inner balloons are often universal; however, their sleeves require different folding and cutting patterns to be hard-set into the actuator construction to achieve tailored motions. Robots with universal pneumatic actuators assembled from a linear series of cylindrical modules with three longitudinal air chambers [10,16,24,25] or a parallel assembly of multi-layer extension actuators [26] have demonstrated capabilities of manipulation or locomotion with their improved universality.

An alternative to the aforementioned bending actuators are soft rotary actuators and soft flexible joints, which can both achieve rotational motion in a compact footprint. This class of actuators may be stacked or used as joints between links. For example, multi-chambered rotary soft pneumatic actuators were developed and characterized in [27]. These rotary actuators are noted to have better bending characteristics than conventional pneumatic networks and can be suitable candidates for active hinges in soft robots. Khin et al. developed fabric-based rotary actuators with flexible hinges and inflatable beams, which enabled the construction of a fabric-based soft robotic arm [28]. Recently, a fiber reinforced flexible joint inspired by arthropods was developed and characterized, which exhibited high force density capabilities compared to base material designs suggesting a need for further development of such actuators [29].

In this study, we developed highly versatile and easily reconfigurable rotary, modular soft robotic actuators. We designed and fabricated inflatable actuators, called unit cells, with an arched reinforcement structure that allows operation with both positive pressure and vacuum. Currently, few such soft rotary actuators or flexible joint actuators exist and even fewer that offer multiple modes of actuation in larger assemblies (i.e., contraction, extension, and bending). Our actuators deviate from traditional bending actuators, due to our design being more similar to the actuators inspired by flexible joints [29] and rotary soft actuators [27,28,30]. This work contributes towards development of enhanced rotary soft actuators by adding modularity, reconfiguration, and structural reinforcement, which may be tuned during design. The attribute of reconfigurability manifests itself through the connection of unit cells in varying orientations. Various unit cell arrangements allow for planar or spatial motions. A corollary arising from the connection scheme is that the proposed soft robotic actuators are able to grow or shrink with the respective addition or removal of unit cells.

Herein, we first present the iterative development of unit cells with the assistance of finite element (FE) analyses to optimize their design and performance. Next, we characterize and discuss the extension, bending, and blocked force response of several connection schemes that varied in total length and orientation. In addition, we experimentally characterize the connection strength and blocking force of individual actuators as well as for linear assembly configurations. Last, we demonstrate applications of our reconfigurable actuators by partitioning a large actuator into two smaller ones to construct a gripper that is able to hold delicate objects, and construct a linear crawling robot to demonstrate how actuators can be reconfigured to develop complex robotic systems.

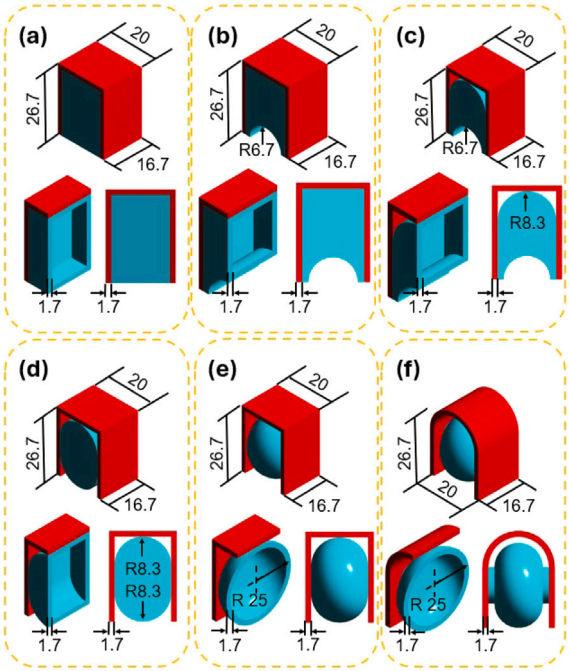

Fig. 1. Dimensioned schematics of select unit cell designs explored in the design process. In all panels, the red region depicts the TPU reinforcement structure, and the other region depicts the internal balloon. All units are in mm. Unit cells in (a)–(e) have the same rectangular reinforcement structure, while (f) introduces an arched structure. Designs in (a)–(c) all have rectangular inner chambers with (a) being a rectangular prism, (b) a rectangular prism with a corrugated base, and (c) adding a rounded top to the internal balloon of design in (b). The shape of the balloon in (d) was cylindrical and (e) was an ellipsoid. In (f) the modified ellipsoid balloon was offset away from the curved part of the reinforcement structure. (For interpretation of the references to color in this figure legend, the reader is referred to the web version of this article.)

2. Methods

2.1. Unit cell design

Unit cells were designed to serve as the building blocks of modular reconfigurable soft robotic actuators that have the ability to achieve several modes of deformation. The unit cells consisted of an inflatable internal balloon that was attached to a flexible structural member (see Fig. 1). The individual unit cells were connected through the sides of the structural members. Internal closed balloons were modeled and fabricated using Elite Double 22 silicone rubber (Zhermack SpA, Badia Polesine (RO), Italy), while the reinforcement structures were additive manufactured using thermoplastic polyurethane (TPU) filament. The unit cells were iteratively designed using the commercially available modeling software SOLIDWORKS and their shape was iteratively optimized through FE simulation.

To study the unit cells' motions and improve their mechanical response, we developed a Lagrangian-based 3D FE model using ANSYS/explicit. Additional details are presented in the forthcoming section. The design goal was to maximize the opening angle of each unit cell and minimize ballooning past the reinforcement structure to constrain the overall width of the unit cells. Our design processes studied the deformation response with various internal balloon geometries, reinforcement structure shapes, and different vertical positioning and offsets of the internal balloon with respect to the reinforcement structure. A concise chronological overview of the explored balloon geometries, reinforcement structures and balloon positioning is shown in Fig. 1. We note here, the balloon material was selected to minimize expansion past the reinforcement structure that may happen with rubbers on the order of hardness from Shore 00–10 to 00–50,

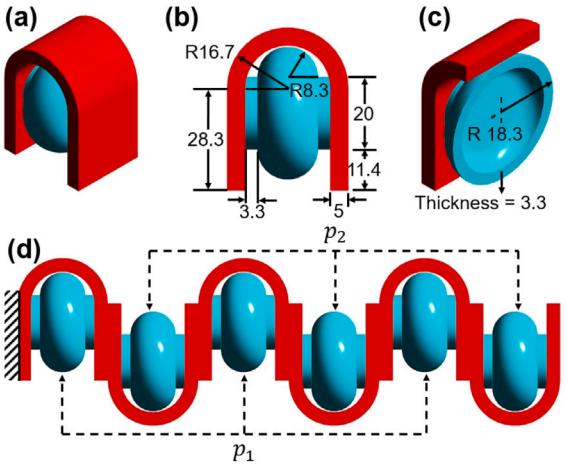

Fig. 2. (a) Shows a 3D isometric view of a single unit cell selected for actuator studies. (b) Shows a dimensioned side view of the unit cell. (c) Shows an isometric view of the sliced unit cell. (d) Shows a representative CAD model of a soft robotic actuator composed of multiple alternating unit cells. All units are in mm.

which were tested in our preliminary material selection. Likewise, the reinforcement structure was designed to be considerably stiffer than the balloon outside of the hinge to promote opening motions, and its thickness was dimensionally constrained to allow for connection holes of adapters that connect the unit cells.

Fig. 1(f) shows our selected unit cell used for further design optimization and exploration. We focused on tuning the thickness of the internal balloon and reinforcement structure. Our unit cell dimensions were not optimized through a rigorous design optimization process, such as topology optimization, and were investigated empirically. Nevertheless, the established dimensions were suitable to achieve desirable motions. We present dimensioned schematics of our finalized unit cell in Fig. 2(a–c).

A schematic of a possible multi-actuator configuration assembled from six unit cells with an alternating orientation is shown in Fig. 2(d). Depending on the applied pressures (p_1 and p_2) in the units cells with the shown orientations, the actuator can exhibit multi-directional bending (case 1 (bending upwards): $p_1 > 0$ and $p_2 \leq 0$) or case 2 (bending downwards): ($p_1 \leq 0$ and $p_2 > 0$), elongation ($p_1 = p_2$ and $p_1 > 0, p_2 > 0$), or contraction ($p_1 = p_2$ and $p_1 < 0, p_2 < 0$). A combination of simultaneously applying positive pressures in both sets of balloons with a pressure differential ($p_1 \neq p_2$) can lead to combined bending and axial motions; which is also true for pressurizing any series of adjacent balloons with a pressure differential (i.e., applying different pressures for each unit cell).

2.2. FE methods

ANSYS/explicit was used in several investigations in this research, in addition to the preliminary development of the unit cells. The material properties of the hyperelastic Zhermack Elite Double 22 silicone rubber and TPU that were used to construct unit cells, were characterized in-house using ASTM D-412 shaped dog bones and 16 mm^3 compression cubes samples. Results of our characterizations are presented in Fig. 3(a) and (b) for the TPU and rubber, respectively. The material properties were defined as *Response function* in ANSYS based on the aforementioned materials data. The reinforcement structure utilized hex-dominated elements (approximately 3200 elements per unit cell), while the more compliant internal balloon uses tetrahedral elements (approximately 32,000 elements per unit cell). A bonded contact was used between each surface. In all simulations, a single fixed support was used on an end of the reinforcement structure. For the initial unit cell design process shown in Fig. 1, all simulations used the

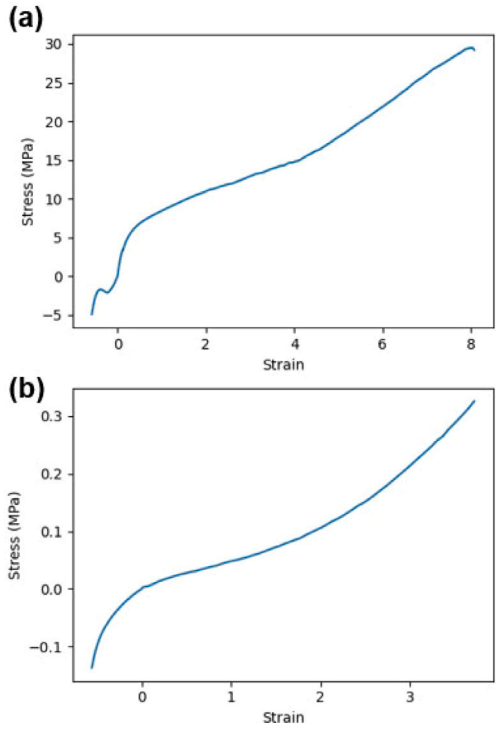

Fig. 3. (a) Shows the full stress–strain response of TPU. (b) Shows the full stress–strain response of Zhermack Elite Double 22 rubber. Strain was computed as the ratio of the change in displacement at the crosshead to the length of the undeformed test specimen.

same pressure ramp up to 0.2 MPa over an interval of 0.2 s and held for 0.8 s with pressure applied normal to the faces of the internal balloons.

2.3. Fabrication

Unit cells were fabricated using a multi-step process as shown in Fig. 4(a–i). The internal balloons were prepared in a two step casting process using manually mixed Zhermack Elite Double 22 silicone rubber, wherein each half was separately cast, and then joined using the same silicone rubber as an adhesive. 2 mm silicone tubing was embedded into each unit cell to allow pressurization. A small air intake valve was utilized in each unit cell to mitigate bursting and air leakage. The internal balloon was joined to the reinforcement structure with a flexible adhesive. Custom male to female connectors were designed to enable connections between unit cells. These connectors were designed to allow various connection configurations but can be used with any unit cell (i.e., the unit cells are universal). An example connector is shown in Fig. 4(j). The flexible reinforcement structures were 3D printed (Creality Ender 3 Pro) using TPU, while the connectors for the unit cells, were 3D printed from polylactic acid (PLA). To assemble actuators, we joined unit cells via the connectors. Note that the connectors do not come in direct contact with the inner balloon, thus preventing the common issue of air leakage associated with mechanical connection. A representative actuator with six unit cells in alternating orientations is shown in Fig. 4(k).

2.4. Experimental methods

2.4.1. Free displacement characterizations

Unit cells and several modular actuators were constructed and experimentally characterized to understand their performance, design considerations, and respective limitations. We conducted experiments to validate the deflections from our FE analyses for both unit cells and for several modular actuators with various connection schemes.

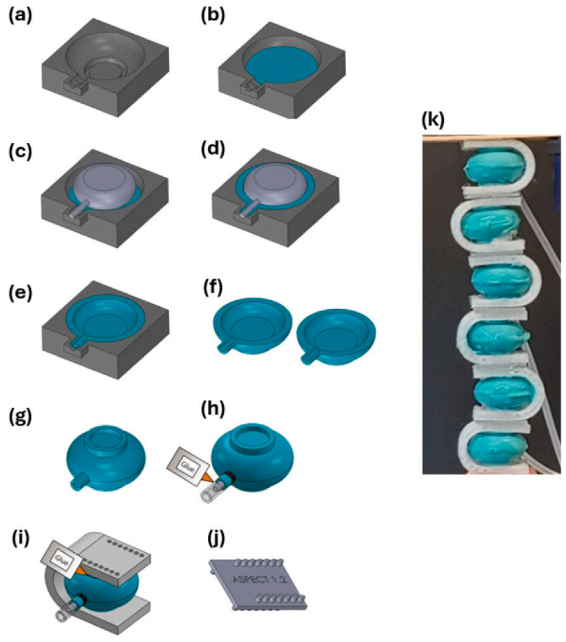

Fig. 4. Overview of the unit cell and actuator construction process. Steps (a)–(e) show the forming of the inner balloon halves shown in (f), and were joined using the silicone rubber as an adhesive in (g). (h) Shows how the PLA intake valve was inserted into the balloon's protrusion and sealed in place using Sil-Poxy™ (Smooth-On, Inc., Macungie, PA, USA). Last, in (i) the balloon was connected to the flexible TPU shell and sealed in place using super glue (Methyl 2-Cyanoacrylate), completing the unit cell. A representative rigid connector is shown in panel (j) which was friction fit into matching holes in the TPU shells. A representative actuator assembled of 6 unit cells with an alternating alignment is shown in (k).

A custom testing apparatus was constructed, ensuring the same fixed-end boundary conditions and sample orientation as the FE simulations. An annotated photograph of the experimental setup for characterizing free displacement is shown in Fig. 5(a). Our test fixture was constructed from linear rails which were mounted to an optical table with custom brackets. A simple pressure control was implemented using an Arduino Mega 2560. The air that was passed into the system was supplied from a building pressure supply (690 kPa). A continuous drive servo was attached to the pressure valve and run for a set time, wherein we consider the final value to characterize motions at a steady internal pressure. A representative pressure plot recorded by the transducer is shown in Fig. 5(b). A block diagram schematic of the air delivery system is shown in Fig. 5(c). We note that the same Arduino is used for data acquisition and servo actuation timing, but we are not using a feedback loop in a classical sense. The unit cells can withstand a maximal pressure of 110 kPa when pressurized for a few seconds, and shorter impulses of higher pressures. The failure behavior of a representative sacrificial unit cell is presented in Figure S1 of the supplementary material file. We selected an inflation pressure of 77 kPa as it allowed us to characterize approximately 70 percent of the pressure range without damaging the unit cells. The spike in measured pressure was due to a sudden increase in pressure that the 0–120 kPa pressure regulator was unable to quickly dissipate, and is why we used a different pressure profile than the unit cell design process. As the trial goes on, the pressure slowly decreases to the nominal pressure of 77 kPa, which was considered in all analyses. Image data were processed using ImageJ to measure deformations. To enable one-to-one comparison with our simulations that accounted for gravity, we recorded an undeformed reference position and use this starting value in our motion analyses.

2.4.2. Blocked force characterization

The maximal force transmission of unit cells was characterized by inflating a triplicate set of unit cells with and without the reinforcement structure in a blocked configuration using the same inflation scheme described in Fig. 5(c). We considered the response of just the inner balloon to study the contribution of the reinforcement structure to force transmission and unit cell efficiency. Unit cells were placed in between the compression platens of a Shimadzu AGS-X load frame equipped with a 10 kN load cell. Pressure and load cell data acquisition were simultaneously triggered and both recorded at a 10 Hz sampling frequency. An annotated photograph of the experimental setup is provided in Fig. 5(d). The same procedure was undertaken to characterize the blocked force characteristics of linear assemblies.

2.4.3. Connection strength characterization

We characterized the connection strength between unit cells for various aspect ratio (AR) of actuator alignments (see details in Section 3.3). Using two unit cells and their respective connectors (for each AR), we utilized a Shimadzu AGS-X load frame to record force and displacement data. An annotated photograph of a sample is shown in Fig. 5(e). Custom attachments were 3D printed from PLA filament and rigidly connected to the ends of the unit cells' reinforcement structures to facilitate tensile load transfer to the load frame. The nominal stiffness of PLA is much greater than TPU, as such we assumed the deformation of the PLA attachments was negligible compared to any structural motions or connection damage. Since we were only interested in the properties of the connection interface, we attached rigid blocks/caps of PLA at the end of the reinforcement structures' openings to prevent the modules from opening during tests.

3. Results

3.1. Unit cell design

Several unit cell designs were explored prior to selecting a single design style for continued development, which was summarized at a high level in Fig. 1. We investigated the impact of geometry on the free-boundary opening of each unit cell shown in Fig. 1, and present results in Fig. 6. We found that rectangular and cylindrical balloons had the worst performance over the entire pressure range, while the corrugated and elliptical balloons performed best. A potential reason is that the edges on the non-elliptical balloons cause uneven pressure distributions compared to elliptical inner balloons and thus elliptical balloons show improved performance. The arched reinforcement structure had the best performance, and led to a notably larger opening angle at lower pressures. While the corrugated balloon designs (Fig. 1(b, c)) slightly outperformed the ellipsoid (Fig. 1(e)), we considered the arched reinforcement structure with the ellipsoidal balloon due to ease of fabrication of the inner cavity in preliminary studies with our fabrication methods. We selected design (f) for continued development as it has the largest opening angle of all of the explored geometries.

3.2. Unit cell response

3.2.1. Deformation of a unit cell

The opening angle of individual unit cells were characterized through simulation and experiments. Comparisons are shown in Fig. 7(a), wherein an experimental photo is shown with the inset (i), and a simulation image is shown in (ii). The opening angle measurement is depicted on the inset (ii). The deformation scale factor of all the FE images in this research is the true deformation scale. Simulations predicted an opening angle, θ, of 34°. Through our experiments on six unit cells, we found an average opening angle of 31.55°, with a standard deviation of 3.02° at 77 kPa. The continuous deformation of the unit cell shows a continuously increasing opening of the unit cell until 35 kPa, followed by a plateau from 35 to 70 kPa, which has a slow increase in pressure. We note that this plateau region has greater radial expansion than the initial inflation region, and may be

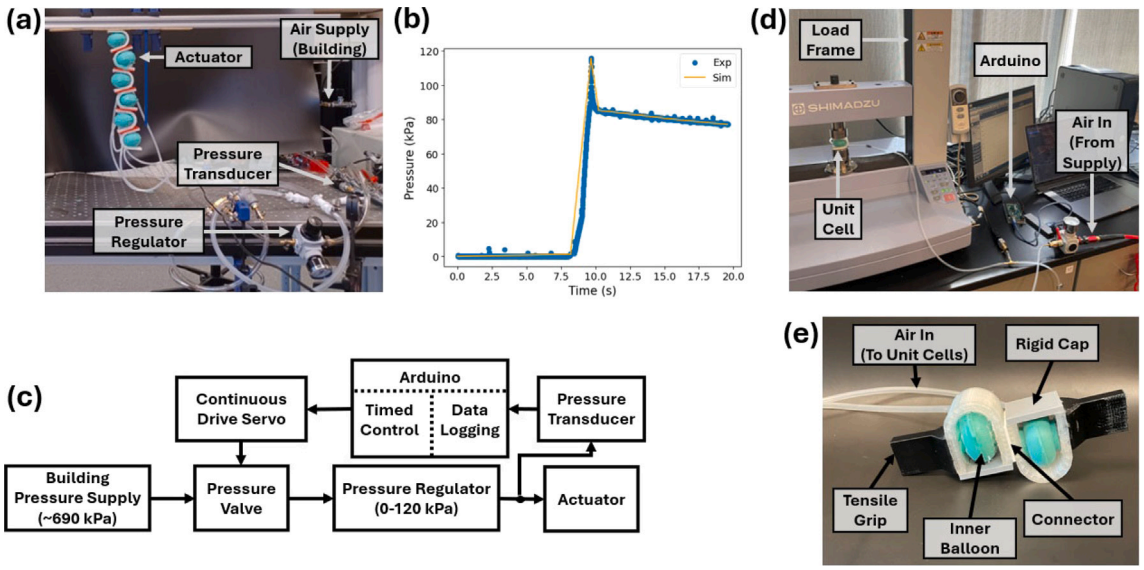

Fig. 5. The experimental setups utilized in this research. (a) Shows an annotated photograph of the experimental setup used to characterize free displacements. A sample pressure plot showing the pressure profile used in simulation (sim) and the corresponding experimental (exp) collected data is shown in panel (b). A block diagram showing the air delivery system is presented in (c). (d) Shows an annotated photograph of the blocked force characterization experimental setup. A representative annotated photograph of a sample for a connection strength test is shown in panel (e).

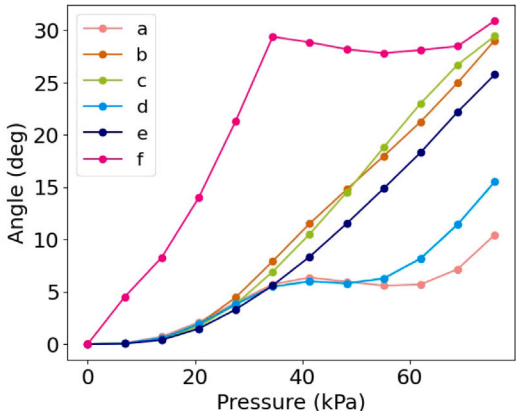

Fig. 6. Simulation results of the designs presented in Fig. 1. The lettering in the legend corresponds to the unit cells presented in Fig. 1.

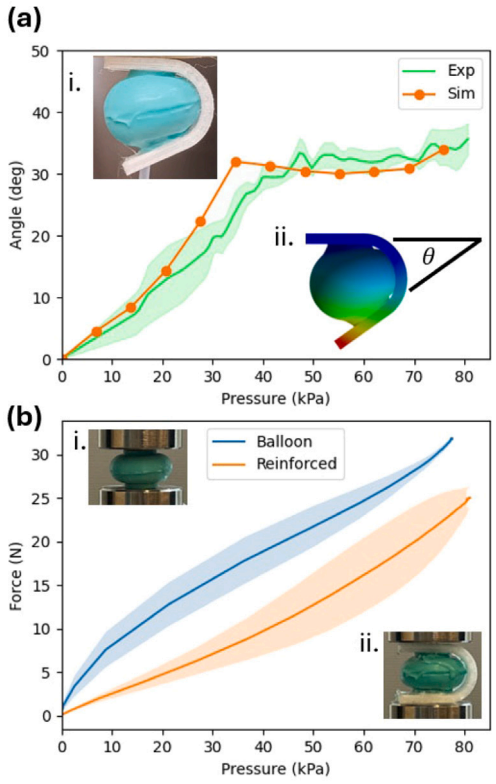

Fig. 7. Experimental characterization of unit cells. (a) Presents a comparison between the experiments and simulations for the relationship of the unit cell opening angle as a function of applied pressure. Bands are for one standard deviation for a set of six unit cells. Images of the unit cell from both experiments (i) and simulations (ii) are shown as insets. (b) Shows a ribbon plot of the blocked force characteristics as a function of pressure for a single unit cell and the internal balloon with the reinforcement structure removed. Bands are for one standard deviation of three tests. Experimental images of an internal balloon and a full unit cell at the start of a test are shown as insets in (i) and (ii), respectively.

partially attributed to the rate of pressurization. The plateau was also observed in other geometries (see Fig. 6 designs a,d). The plateau response was likely attributed to large strains accumulating in the hinge material that the balloon must overcome by performing a sufficient amount of work. While the physical unit cells generally burst at around 110 kPa, additional simulations were performed to investigate the opening response of unit cells at much higher pressures, which is described in more detail in Section 2 of the supplementary material. These simulations show that the unit cells continue to open after 70 kPa before plateauing again with an opening angle of 63° at 137 kPa. The agreement between simulations and experiments in Fig. 7(a) shows our fabrication and testing methods were repeatable. In addition, our simulation model was in good agreement with our experimental results, which enabled computational studies on multi-celled assemblies.

3.2.2. Blocked force of a unit cell

We characterized the blocked force of unit cells with and without the reinforcement structure. Experimental results are shown in Fig. 7(b). The reinforcement structure leads to lower force transmission upon pressurization compared to the inner balloon without the

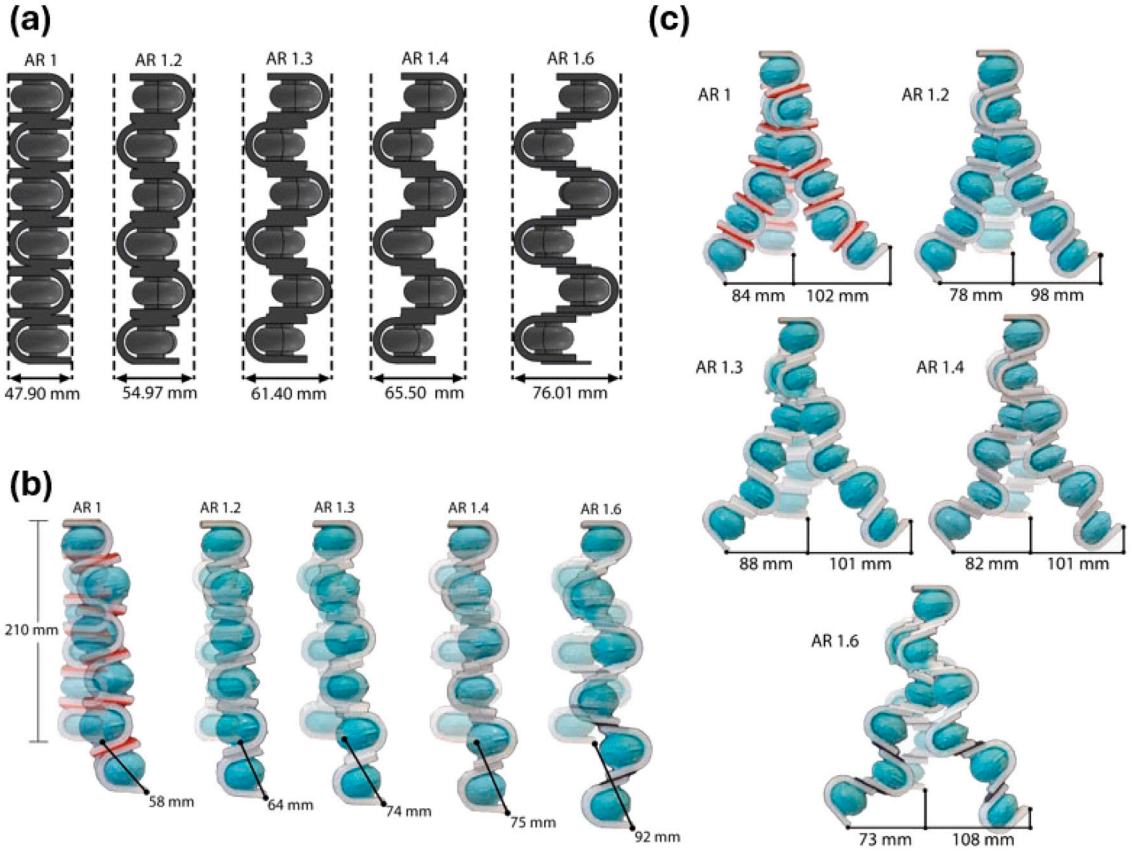

Fig. 8. Characterizing actuators constructed with different aspect ratios. (a) Shows CAD renderings of each AR with alternating alignments used in this section of the study. (b) Examines the extensile response for all AR by overlaying photographs of the actuators in deformed and undeformed states. Extension was measured from the undeformed tip of the actuator to the deformed tip and includes deformation due to gravity. Left and right bending are shown for all AR in (c). Bending was measured from the undeformed tip of the actuator to the deformed tip, and is in units of mm. Only the displacement in the horizontal direction was measured for bending.

reinforcement structure. This is attributed to the structural stiffness resisting the work being done by the balloon. Additional commentary is provided in the Discussion section.

3.3. Affect of aspect ratio on motion

The utility of the unit cell approach is that it can be leveraged to design modular soft robots that can achieve several types of motion using universal modules. We investigated through simulation and experiments, how actuator responses vary when the centers of the unit cells (defined at the center of the ellipsoidal internal balloons) are misaligned. Actuators were constructed from six unit cells with the designs shown in Fig. 8(a). For each design, we investigated the steady-state displacement per our experimental protocol. Experimental images of representative trials with marked displacements are shown in Fig. 8(b) and (c), for extension and bending, respectively.

Fig. 8(b) shows notable differences in extension with variation of the AR parameter, with a 6 mm difference between an AR of 1 and 1.2, and a 10 mm difference between an AR of 1.2 and 1.3. We attribute the lack of change between an AR of 1.3 and 1.4 to possible manufacturing issues.

Simulation results are directly compared with experimental data in Fig. 9. Comparisons of the representative experimental and simulation images for an actuator with AR = 1.3 are shown for the extension, left bending, and right bending in panels (a), (c), and (e), respectively. The maximal standard deviation across all AR for extension, left bending and right bending, is 3 mm, 1.78 mm, and 2.87 mm, respectively, suggesting good repeatability. Both experimental and simulation results show agreement that an increase in AR leads to an increase in extensile motions. Interestingly, neither experimental nor simulation results show any clear relationship between AR and bending motions. The bending of an actuator with AR = 1.3 outperforms most others in simulation and experiments except the right bending experimental results. We note that the right bending was significantly larger than the left bending. The magnitude of the bending motion was closely correlated to both the orientation of the unit cell at the fixed boundary, and the inflation sequence of the unit cells. In the right bending case, the unit cell at the boundary was inflated and scaled the motion of the remaining five. However, in left bending, the boundary unit cell was not inflated and instead the second unit cell was inflated, which only scaled the motions of the next four unit cells. During extension, the pairs of inflated unit cells cancel the opening angles in each direction resulting in a pure linear extension. However, the first unit that is attached to the fixed end can only open relative to that fixed surface, which governs the resulting right offset of the total deformation as observed in the extension results as well as the difference between the left and right bending. This phenomena occurred throughout the span of each linear assembly and should be considered when designing these actuators from unit cells.

3.3.1. Affect of AR on connection strength

We characterized the connection strength for each AR between two unit cells. We considered all AR as the connections resistance to motion will change based on the amount of overlap between the connectors and the locations of localized forces. Experimental characterizations are provided in Fig. 10. The results at low displacements show an increase in measured forces as the AR increases. As displacements increase

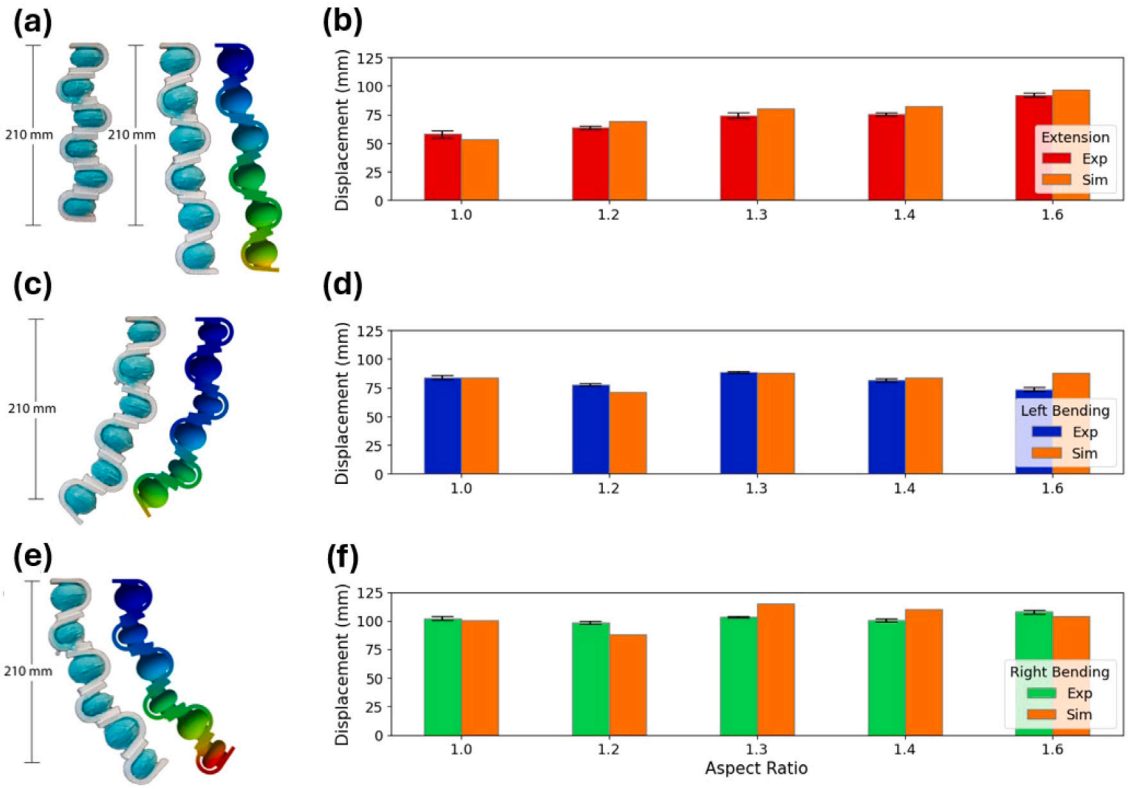

Fig. 9. Comparison between experimental and simulation results for extension, left bending, and right bending. Experimental images are shown beside simulation contours for an AR of 1.3 in panels (a), (c), and (e) for extension, left bending, and right bending, respectively. Bar charts for all AR are shown in (b), (d), and (f) where (b) shows extension, (d) shows left bending, and (f) shows right bending. Bending was measured from the undeformed tip to the deformed tip in either case. Only displacement in the horizontal direction was measured for bending.

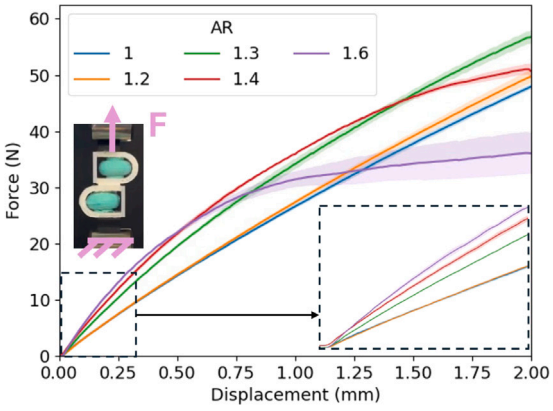

Fig. 10. Experimental characterization of the connection strength between unit cells for each examined AR. Bands are for one standard deviation over an average of three tests. To better visualize the initial forces, a zoomed-in inset plot is shown for the force displacement response over the dashed domain and range. An experimental image with the direction of applied force is shown as an inset.

beyond 0.5 mm, a reduction in resistance to motion is observed with the increase of AR that is a function of displacement. The underlying causes and implications are outlined in the discussions.

3.4. Alternating vs. Matching configurations

In addition to alternating configurations, matching configurations (where unit cells all face the same direction) are an equally valid connection scheme with our common pin connectors. We investigated a matching configuration design with an overlapping connection as shown in Fig. 11(a). Due to the unit cells having the same orientation, applying positive pressure to all of the unit cells will cause bending motions. A side-by-side image comparison of the experimental and simulation results is presented in Fig. 11(b) and (c), respectively. In addition, we compared the right bending motions of this actuator with an alternating alignment with AR = 1 (identical alignment to the matching configuration) and 1.6 (exhibited maximum right bending) through simulations and experiments as shown in Fig. 11(d). The results show that the actuators with a matching alignment have a 225.8% increase in bending motions compared to the alternating configuration of AR 1.6, and a 233.1% increase in bending motions compared to the alternating configuration of AR 1. We note, that there was greater discrepancy between the experimental and simulation results for the matching configuration. However, the overall improvement in performance was still reflected in the experimental data with high repeatability.

3.5. Actuator length

3.5.1. Deformation

We examined the affect of the addition of unit cells on extensile motions for actuators with an alternating unit cell configuration to observe the underlaying relationship. Specifically, we examined the deflections at a steady internal pressure of 77 kPa. Our scope was restricted to actuators with an AR of 1, with two, four and six unit cells as shown in Fig. 12(a–c), respectively. A summary of our experimental and simulation results is presented in Fig. 12(d). Experimental results show a consistent increase in the extensile response with the addition of unit cells. This was not always mirrored in the simulations, and is discussed in Section 4.

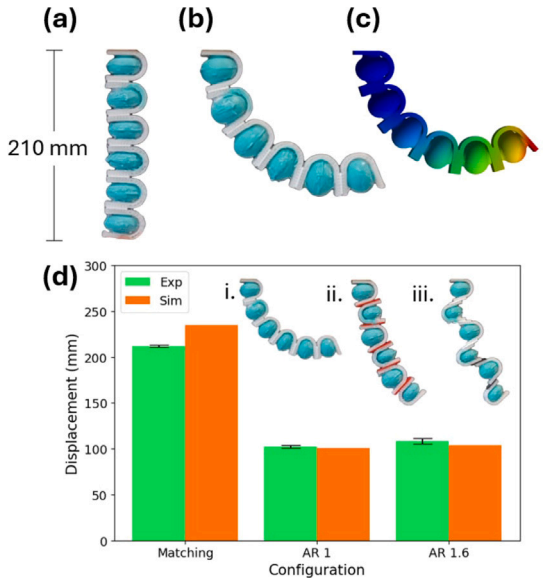

Fig. 11. Examining the deformation of actuators with a matching unit cell configuration. (a) Shows an actuator constructed with unit cells with overlapping centers of the elliptical inner balloons opening in the same direction (i.e., a matching configuration). An experimental image of the matching configuration actuator at 77 kPa is shown in (b) and FE simulation results are shown in (c). (d) Shows a bar chart comparing the right bending of a matching alignment with an actuator with an AR of 1 and 1.6. Error bars represent one standard deviation. The matching and alternating actuators with an AR of 1 and 1.6 at 77 kPa are shown as insets in (i), (ii), and (iii), respectively.

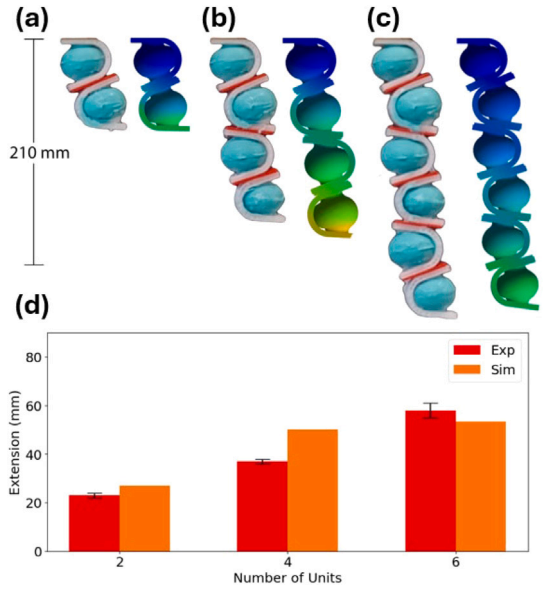

Fig. 12. Shows experimental and simulation results for extensile deformation for alternating configuration actuators with (a) two, (b) four, and (c) six units with an AR of 1. Extension was measured as the distance from the undeformed tip to the deformed tip. A summary bar chart is presented in (d). Error bars represent one standard deviation.

3.5.2. Blocked force

The blocked force of actuators with both matching and alternating (AR = 1.2) configurations were experimentally characterized. We considered actuators with two, four, and six unit cells. We selected AR = 1.2, as it is nearly dimensionally identical to flipping the orientation of a matching connector. Axial blocked force results are presented in Fig. 13 with the matching configurations in (a), and the alternating

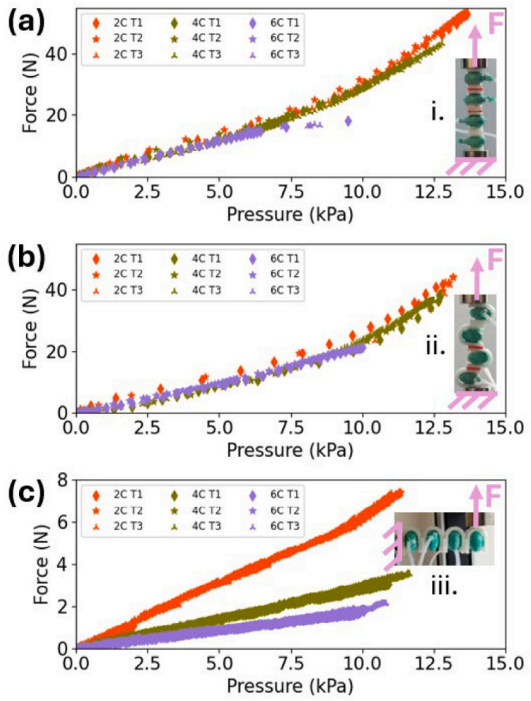

Fig. 13. Shows experimental results for the blocked force response of actuators with two, four, and six units. (a) Shows the blocked axial force of actuators with a matching configuration. (b) Shows the blocked axial force of alternating actuators (AR = 1.2). We show the blocked bending force of a matching configuration actuator in (c). Representative actuators at the start of a test are shown in insets (i), (ii), and (iii), for panels (a), (b), and (c), respectively.

configurations in (b). The matched configuration blocked bending force is shown in (c). We only characterized the matching configuration because the alternating configurations exhibit smaller bending and are less suitable to be used in assemblies as grippers. In addition, the alternating configurations are likely significantly more compliant than matching configurations when subjected to bending loads due to the lower stiffness contributions of the unactuated cells. Representative actuators during a test are shown as insets (i), (ii), and (iii) for panels (a), (b), and (c), respectively.

3.6. Applications

3.6.1. Grasping fragile objects

A common application of soft robotics is grasping delicate objects such as food. To demonstrate the reconfigurability of our unit cells for on-demand tasks, we reconfigured a six unit cell actuator into two smaller three-unit celled actuators with a matching configuration. Experimental photographs are provided in Fig. 14(a) and (b) for the pressurized and unpressurized actuator states, respectively. To facilitate gripping, we applied a rubber pad to the tip of the most distal unit cell. Our actuators were able to hold an orange (210 g), a banana (182 g), an apple (130 g), and an uncooked egg (60 g) as shown in Fig. 14(c–f), respectively.

3.6.2. Locomotion

Another common application of a soft robot is locomotion as shown in Fig. 15(a). To demonstrate this possible use of the proposed actuators, we constructed a linear assembly of three unit cells with an alternating configuration using the AR = 1 and AR = 1.2 connectors, and studied the assembly's forward motions. We flipped the AR = 1 connection to pitch the front of the robot to help facilitate linear motions. A small strip of sandpaper was added to the base of the most

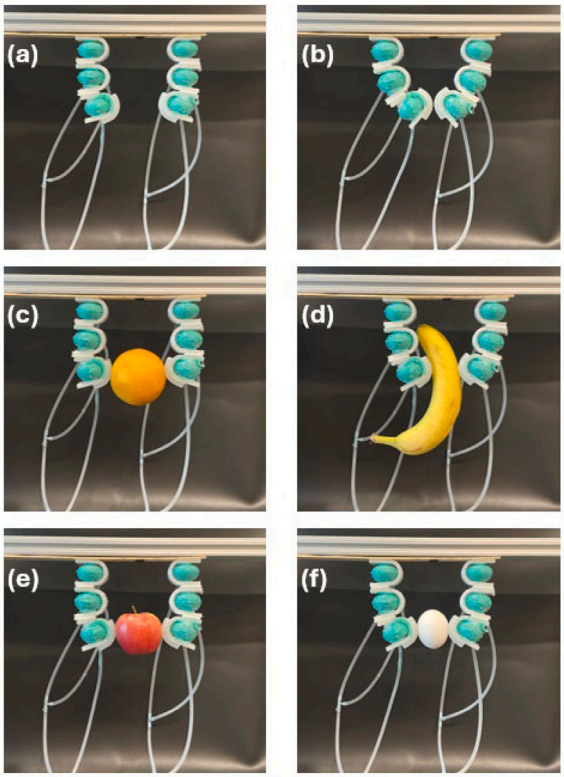

Fig. 14. Six celled actuators are reconfigured into two three-unit celled actuators with a matching configuration. (a) Shows the actuators when unpressurized, while (b) shows the actuators when pressurized. We demonstrate the actuators can grasp several delicate objects such as an orange (c), a banana (d), an apple (e), and an uncooked egg (f), without damaging them. (For interpretation of the references to color in this figure legend, the reader is referred to the web version of this article.)

forward unit cell to help control the slipping at the ground contact. The robot was approximately 110 mm in length.

The time history of motion presented in Fig. 15(a) is contained within the time span of the single stride marked in Fig. 15(b). The full time span contained ten strides, all of which were driven by 70 kPa of pressurization to the central unit cell. For the nine strides following the marked single stride, cells were continuously pressurized to 70 kPa and depressurized. At t = 0 s and t = 2.53 s, the robot was not in motion. At t = 2.07 s the central unit cell was expanding, and at t = 2.20 s the central cell was depressurizing. The inflation of the central unit cell propelled the most forward cell aided by the pitch induced by the connector. When depressurization happened, the sandpaper increased contact friction, and the rear unit cell squeezed towards the front and center cells. Over ten strides the robot displaced 133.93 mm and moved approximately 11.9% of its body length per stride. We note that there likely exists more optimal gaits and connection schemes. However, these results demonstrate the versatility of the proposed actuators for complex tasks such as locomotion.

4. Discussion

A unit cell design and fabrication scheme amendable to the construction of reconfigurable modular soft robotic actuators was presented. We demonstrated that the response of actuators was not only dependent on the unit cell geometry, but heavily dependent on unit cell connection orientation and height. The forthcoming subsections discuss our key findings in detail and their broader implications for this actuator class.

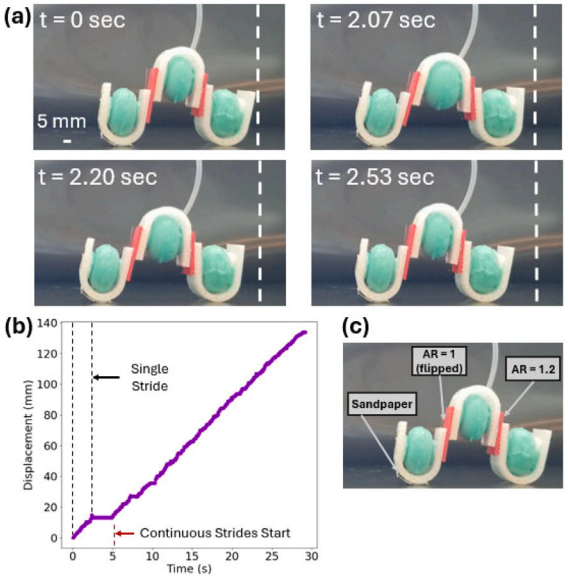

Fig. 15. Three unit cells were reconfigured to realize a linear crawling robot. (a) Shows photographs of key time steps within a single stride of the linear crawling robot. (b) Presents the robot displacement as a function of time. We isolated the first stride which corresponds with the snapshots presented in panel (a). An annotated photograph of the robot is presented in (c).

4.1. Experimental and simulation trends in actuation

4.1.1. The reinforcement structure lowers force transmission

Fig. 7(b) showed that the reinforcement structure lowers the force transmission in a blocked configuration, compared to the inner balloon without the structure. As mentioned, when balloon inflates it must overcome the opposing forces and moments from the hinge joint reinforcement structure. When only considering the balloon, the change in force transmission is visibly higher at lower pressures, compared to the almost linear relationship for the whole unit cell. For pressures above 40 kPa, the response of the balloon and unit cell becomes similar with an offset that might represent the energy loss due to the stiffness of the reinforcement structure. Aside from containing the balloons expansion and providing a medium for our connection scheme, it is clear that the reinforcement structure significantly affects the actuator efficiency. While the reduction in force transmission and associated inefficiency is undesirable, the force response is largely preserved. As such, future work should explore improved structural design of reinforcement structure to maximize the efficiency.

4.1.2. Extension increases with aspect ratio for an alternating configuration

We observed in both simulations and experiments that the alternating configurations of the actuator with six units showed greater extension when a greater AR was used (see Fig. 9). Each unit cell had a similar opening angle, however, the actuator misalignment causes a scaled offset to the adjacent cells' motions, which varies as a function of AR. This was considered in the initial design phase and was a motivating reason that AR was varied.

4.1.3. Bending has no obvious correlation with aspect ratio for alternating configurations

The simulation and experimental results of bending show good agreement for most cases; except in the case of left bending for AR 1.6 and right bending for AR 1.3 and 1.4. The differences between simulation and experiments can likely be explained by differences in the individual unit cells, which are quantitatively observed by the variation of opening angles with free-boundary inflation in Fig. 7(a).

Imperfections in unit cell fabrication at the TPU-balloon interface and in the microstructure of the TPU may have contributed to results variability, and are known fabrication limitations. In addition, layer delamination is possible at high unit cell pressures, even though it was not observed. We provide a figure of a representative balloon-structure interface in the supplementary material, along with a brief discussion to describe how the joining processes may lead to variability.

Although the largest bending was observed in AR 1.3 and smallest in AR 1.2, in both simulations and experiments, we were unable to identify a clear correlation between AR and bending. Seemingly consistent displacements led us away from further explorations investigating intermittent AR or examining a curve fit. We note that it is possible that unit cell pairs cancel out the offset associated with AR that occurs with actuation in the adjacent unit cells, as the opening angles of the units or unit pairs do not change with changes in the AR. It is more likely, however, that the variables are not directly linked and other factors such as mass, and most importantly, the deflection of non-inflated units in the left and right bending of alternating configurations influence the performance. Note that in the left and right bending experiments, pressure was only supplied to *every other unit cell*. While providing vacuum to the units to enable contraction was out of the scope of this paper, it could be performed as part of the future studies to validate the potential improved performance of such configurations.

4.1.4. The AR changes connection strength

Connections with lower AR are able to withstand larger overall displacements perpendicular to the connectors, however, they resist motion with less force at lower displacements as shown in Fig. 10. This means that these connections will begin to separate at lower perpendicular loads compared to the high AR connections, but hold their connection longer and stronger. High AR connections require more force to initiate separation, likely arising from moment arms and off axis forces forming at the connection interface due to the non-concentric loading. However, these connections tend to begin detaching at lower displacements at an off angle from the axis of applied loading as signaled by the reduction in force at larger displacements.

4.1.5. A matching configuration displays greater bending displacement

As expected, a matching configuration displayed greater bending displacements than the alternating configurations as shown in Fig. 11. Since there are more unit cells contributing to the bending action in the matching configuration than for the alternating configuration, it is obvious to expect a greater bending displacement. The trade-off of the matching configuration is in its inability to bend in the opposite direction or to perform extensile behavior. The benefit of modularity in the system, however, is that it allows for this configuration to be reassembled without adding more units if greater bending displacement is desired.

4.1.6. Extension increases with number of units for an alternating configuration

The system was designed to be modular in part so that more unit cells could be added if the application required them. We added unit cells to an alternating configuration with AR 1 as shown in Fig. 12. We observed that extension increased non-proportionally as we added more unit cells. The simulations showed that the difference in extension between 4 and 6 units was not significant, but this was contradicted by experiments which show an increase of 56% between the addition of new units. All of the factors discussed in Section 4.1.3 are relevant here to explain the difference between experiments and simulations.

4.1.7. Actuator length has different effects on the blocked axial and bending force response

In Fig. 13 we observed that the actuator length has no discernible impact on the axial force transmission characteristics in either configuration, and the magnitude of force transmission is similar between the two configuration types. Longer actuators buckle at significantly lower pressures, which may limit their general usage. However, the bending force is significantly reduced as the actuator grows in length. Presumably due to a decrease in bending stiffness as the length increases.

4.2. Reconfiguring actuators for on-demand tasks

A key benefit of our actuators is that we are able to change our configuration space on-demand for optimal execution of a task. In Fig. 14, we demonstrated the reconfigurability of actuators for on-demand tasks, and their ability to grasp fragile objects without damaging them. In a matching configuration, it is easier to achieve large bending angles with less actuators. Most importantly, we are able to swap directly between a single actuator with an AR of 1 to this two actuator system with matching configurations, without the need to fabricate new parts. Likewise, in Fig. 15, we demonstrated that these actuators can be used for more complex tasks such as locomotion.

Our results concerning assemblies have exclusively focused on the construction of linear assemblies with planar motions. Construction of connectors which have rotated orientations of pins on each side of the connectors would facilitate the construction of assemblies which can exhibit spatial motions. For brevity, we have not systematically explored the full range of off-angle connection schemes and their alignment. Particularly because such connection schemes are significantly less restricted and are better suited for application specific investigations. However, to show enabled spatial configuration capabilities, we provide photographs of four assemblies constructed from connectors with 90° offset pins inflated to 77 kPa in Figure S4 of the Supplementary Material that demonstrate the possibility of spatial motions.

5. Conclusions and future work

A unit cell design approach was taken to conceptualize and fabricate reconfigurable modular soft robotic actuators that can achieve tailored motions with various connection schemes. The main conceptual contribution of this work lies in the idea of connecting universal rotary soft actuators (unit cells) through connectors with a universal mechanical interface. Furthermore, offsetting and tuning actuator alignment relative to an axis of symmetry in a modular soft robotic system can lead to substantial changes in mechanical performance. Another key benefit of our actuators is that we are able to change our task space on-demand for optimal execution of a task.

We developed and characterized individual unit cells consisting of an inflatable balloon attached to an arched reinforcement structure that operate by bending upon inflation. The opening angle and blocked force response of individual unit cells selected for designs were quantified and discussed. The offset of adjacent unit cells relative to the balloon centers in alternating configurations and their effect on the extensile and bending response of the actuator were quantified using FE and experimental analyses. We showed that increasing the so-called aspect ratio leads to improved extensile response, but there was no discernible correlation with bending motions. The aspect ratio was also shown to strongly contribute to connection strength, when the actuators were loaded perpendicular to the interface. In addition to alternating configurations, we showed that matching configurations have an improved bending response, at the cost of modulating directional motion through selective unit cell pressurization. We also showed actuator length does not change the blocked axial force response, but dramatically reduces the blocked bending response of actuators. Last, we demonstrated these

actuators can be used for tasks such as delicate food handling and the constructing of a linear crawling robot with a simple reconfiguration.

Future improvements may be made to the experimental and fabrication methods by developing improved joining techniques or exploring more concise manufacturing processes, such as lost materials methods or additive manufacturing the entire unit cell in a single step. Last, future work may continue to investigate how to optimally arrange unit cells to construct reconfigurable soft robotic systems that enable improved locomotion and complex spatial motions.

Funding

This material is based upon work supported by the National Science Foundation, United States under Grant No. 2235647.

CRediT authorship contribution statement

Nicholas Pagliocca: Writing – original draft, Visualization, Validation, Investigation, Formal analysis, Data curation, Methodology, Software. **Aatish Gupta:** Visualization, Methodology, Investigation. **Joshua Knospler:** Investigation, Validation. **Nand K. Singh:** Visualization, Methodology, Investigation, Conceptualization. **Mitja Trkov:** Writing – review & editing, Supervision, Resources, Project administration, Funding acquisition, Conceptualization.

Declaration of competing interest

The authors declare that they have no known competing financial interests or personal relationships that could have appeared to influence the work reported in this paper.

Data availability

Data will be made available on request.

Appendix A. Supplementary data

Supplementary material related to this article can be found online at https://doi.org/10.1016/j.sna.2024.115830.

References

[1] J. Shintake, V. Cacucciolo, D. Floreano, H. Shea, Soft robotic grippers, Adv. Mater. (Weinheim) 30 (29) (2018) e1707035–n/a.
[2] K.C. Galloway, K.P. Becker, B. Phillips, J. Kirby, S. Licht, D. Tchernov, R.J. Wood, D.F. Gruber, Soft robotic grippers for biological sampling on deep reefs, Soft Robot. 3 (1) (2016) 23–33.
[3] T. Ranzani, M. Cianchetti, G. Gerboni, I. De Falco, A. Menciassi, A soft modular manipulator for minimally invasive surgery: Design and characterization of a single module, IEEE Trans. Robot. 32 (1) (2016) 187–200.
[4] M. Runciman, A. Darzi, G.P. Mylonas, Soft robotics in minimally invasive surgery, Soft Robot. 6 (4) (2019) 423–443.
[5] L. Wang, G. Peng, W. Yao, S. Biggar, C. Hu, X. Yin, Y. Fan, Soft robotics for hand rehabilitation, in: Intelligent Biomechatronics in Neurorehabilitation, Elsevier, 2020, pp. 167–176.
[6] M. Raeisinezhad, N. Pagliocca, B. Koohbor, M. Trkov, Design optimization of a pneumatic soft robotic actuator using model-based optimization and deep reinforcement learning, Front. Robot. AI 8 (2021) http://dx.doi.org/10.3389/frobt.2021.639102.
[7] V. Oguntosin, A. Akindele, Design and characterization of artificial muscles from wedge-like pneumatic soft modules, Sensors Actuators A: Phys. 297 (2019) 111523, http://dx.doi.org/10.1016/j.sna.2019.07.047.
[8] J. Seo, J. Paik, M. Yim, Modular reconfigurable robotics, Annu. Rev. Control Robot. Auton. Syst. 2 (2019) 63–88.
[9] C. Zhang, P. Zhu, Y. Lin, Z. Jiao, J. Zou, Modular soft robotics: Modular units, connection mechanisms, and applications, Adv. Intell. Syst. 2 (6) (2020) 1900166.
[10] B. Zhang, C. Hu, P. Yang, Z. Liao, H. Liao, Design and modularization of multi-DoF soft robotic actuators, IEEE Robot. Autom. Lett. 4 (3) (2019) 2645–2652.
[11] J. Zou, Y. Lin, C. Ji, H. Yang, A reconfigurable omnidirectional soft robot based on caterpillar locomotion, Soft Robot. 5 (2) (2018) 164–174, http://dx.doi.org/10.1089/soro.2017.0008.
[12] Z. Liu, Y. Wang, J. Wang, Y. Fei, Design and locomotion analysis of modular soft robot, Robotica 40 (11) (2022) 3995–4010, http://dx.doi.org/10.1017/S0263574722000728.
[13] G. Agarwal, M.A. Robertson, H. Sonar, J. Paik, Design and computational modeling of a modular, compliant robotic assembly for human lumbar unit and spinal cord assistance, Sci. Rep. 7 (1) (2017) 14391.
[14] J. Ogawa, T. Mori, Y. Watanabe, M. Kawakami, M.N.I. Shiblee, H. Furukawa, MORI-A: Soft vacuum-actuated module with 3D-printable deformation structure, IEEE Robot. Autom. Lett. 7 (2) (2022) 2495–2502.
[15] Z. Jiao, C. Ji, J. Zou, H. Yang, M. Pan, Vacuum-powered soft pneumatic twisting actuators to empower new capabilities for soft robots, Adv. Mater. Technol. 4 (1) (2019) 1800429.
[16] Y. Zhang, T. Zheng, J. Fan, G. Li, Y. Zhu, J. Zhao, Nonlinear modeling and docking tests of a soft modular robot, IEEE Access 7 (2018) 11328–11337.
[17] Z. Jiao, C. Zhang, W. Wang, M. Pan, H. Yang, J. Zou, Advanced artificial muscle for flexible material-based reconfigurable soft robots, Adv. Sci. 6 (21) (2019) 1901371.
[18] J. Legrand, S. Terryn, E. Roels, B. Vanderborght, Reconfigurable, multi-material, voxel-based soft robots, IEEE Robot. Autom. Lett. 8 (3) (2023) 1255–1262.
[19] J.-Y. Lee, W.-B. Kim, W.-Y. Choi, K.-J. Cho, Soft robotic blocks: Introducing SoBL, a fast-build modularized design block, IEEE Robot. Autom. Mag. 23 (3) (2016) 30–41.
[20] H. Yang, S. Jin, W.D. Wang, Modular assembly of soft machines via multidirectional reclosable fasteners, Adv. Intell. Syst. 4 (7) (2022) 2200048.
[21] S. Kurumaya, B.T. Phillips, K.P. Becker, M.H. Rosen, D.F. Gruber, K.C. Galloway, K. Suzumori, R.J. Wood, A modular soft robotic wrist for underwater manipulation, Soft Robot. 5 (4) (2018) 399–409, http://dx.doi.org/10.1089/soro.2017.0097.
[22] T. Jin, T. Wang, Q. Xiong, Y. Tian, L. Li, Q. Zhang, C.-H. Yeow, Modular soft robot with origami skin for versatile applications, Soft Robot. 10 (4) (2023) 785–796, http://dx.doi.org/10.1089/soro.2022.0064.
[23] N. Pagliocca, M. Trkov, B. Koohbor, Modular soft robotic actuators from flexible perforated sheets, Adv. Eng. Mater. 25 (19) (2023) http://dx.doi.org/10.1002/adem.202300583.
[24] T. Ranzani, M. Cianchetti, G. Gerboni, I.D. Falco, A. Menciassi, A soft modular manipulator for minimally invasive surgery: Design and characterization of a single module, IEEE Trans. Robot. 32 (1) (2016) 187–200, http://dx.doi.org/10.1109/TRO.2015.2507160.
[25] M.A. Robertson, P. Jamie, New soft robots really suck: Vacuum-powered systems empower diverse capabilities, Science Robotics 2 (9) (2017) eaan6357, http://dx.doi.org/10.1126/scirobotics.aan6357, arXiv:https://www.science.org/doi/pdf/10.1126/scirobotics.aan6357.
[26] J.W. Ambrose, N.Z.R. Chiang, D.S.Y. Cheah, C.-H. Yeow, Compact multilayer extension actuators for reconfigurable soft robots, Soft Robot. 10 (2) (2023) 301–313, http://dx.doi.org/10.1089/soro.2022.0042.
[27] Y. Sun, Y.S. Song, J. Paik, Characterization of silicone rubber based soft pneumatic actuators, in: 2013 IEEE/RSJ International Conference on Intelligent Robots and Systems, Ieee, 2013, pp. 4446–4453.
[28] P.M. Khin, J.H. Low, M.H. Ang Jr., C.-H. Yeow, Shape programming using triangular and rectangular soft robot primitives, Micromachines (Basel) 10 (4) (2019) 236, http://dx.doi.org/10.3390/mi10040236.
[29] M. Xu, G. Wang, C. Rong, Fiber-reinforced flexible joint actuator for soft arthropod robots, Sensors Actuators A 340 (2022) 113522, http://dx.doi.org/10.1016/j.sna.2022.113522.
[30] J. Fras, Y. Noh, H. Wurdemann, K. Althoefer, Soft fluidic rotary actuator with improved actuation properties, in: 2017 IEEE/RSJ International Conference on Intelligent Robots and Systems, IROS, IEEE, 2017, pp. 5610–5615.

Nicholas Pagliocca received his B.S. and M.S. in Mechanical Engineering from Rowan University, Glassboro, NJ, USA in 2020 and 2022, respectively. His master's thesis research focused on the design and control of modular soft robotic actuators with architected structures. His research interests include functional materials, metamaterials, sensors and actuators, system identification, modular and reconfigurable robots, and soft robotics.

Aatish Gupta received his B.S. in Mechanical Engineering from Rowan University, Glassboro, NJ, USA and performed this research during his studies at Rowan. He is currently working towards his master's degree at Carnegie Mellon University. He is working on a master's thesis focused on path planning for mobile robotics. His research interests include mechanical design, mobile robotics, and robotics for manufacturing.

Joshua Knospler received his B.S. in Mechanical Engineering from Rowan University, Glassboro, NJ, USA. He is currently working towards his master's thesis at Rowan University. His research interests include mechanical design, modular and reconfigurable robots, and soft robotics.

Nand K. Singh received a B. Tech degree in Mechanical Engineering from West Bengal University of Technology, India in 2011 and a Ph.D. degree in Mechanical Engineering from the Indian Institute of Technology, Dhanbad, India in 2016. He was an assistant professor for three years in India then moved to Rowan University, USA as a postdoctoral research associate, 2019–2021. After 2021 he was promoted and assigned responsibility for independent teaching and research at Rowan University. His research interests include composite materials, additive manufacturing, and designing and characterization of metamaterials.

Mitja Trkov received a B.S. degree in Mechanical Engineering from the University of Ljubljana, Slovenia in 2007 and the Ph.D. degree in Mechanical and Aerospace Engineering from Rutgers University, Piscataway, NJ, USA, in 2016. He was a postdoctoral research fellow in Mechanical Engineering with the University of Utah, Salt Lake City, UT, USA. His research interests include human-machine interactions, robotics, system dynamics and control, mechatronics, and biomechanics with applications in biomedical engineering, autonomous systems, and civil engineering.